MODELLING, CONTROL AND APPLICATION OF DYNAMIC PROGRAMMING TO A SERIES-PARALLEL HYBRID ELECTRIC VEHICLE

Ivan Miguel Trindade[(a)], Agenor de Toledo Fleury[(b)]

[(a),(b)] Mechanical Engineering Department, Polytechnic School, University of Sao Paulo, Brazil
[(b)] Mechanical Engineering Department, FEI University, Sao Bernardo do Campo, Brazil

[(a)]ivan.trindade@usp.br, [(b)] agfleury@fei.edu.br

ABSTRACT
Hybrid Electric Vehicles (HEVs) present a wide range of powertrain configurations, degrees of hybridization and added costs when compared to conventional powertrains. From the point of view of control system, the major problem is the reduction of fuel consumption and pollutant emission. A method for determining the strategy that best suits this problem relies on minimization methods that find the optimal control variables depending on the system states and cost functions.
This paper presents the modelling of the powertrain of a series-parallel HEV and control strategies with focus on fuel consumption reduction. As energy management strategy, a rule based (sub optimal) and dynamic programming (optimal) methods were implemented. Results obtained with both models are compared with real dynamometer test.

Keywords: hybrid electric vehicle, dynamic programming, fuel consumption, optimization

1. INTRODUCTION

The major powertrain losses in a conventional vehicle are inherited by the relatively low average fuel efficiency of combustion engines (around 33% for spark ignited) and the very low efficiency at part loads, typical of operation in urban driving cycles. On the other hand, an electric vehicle (EV) provides high energy conversion efficiency when combining battery, electric motor and motor electronics which can be as high as 80% for the complete power path. The main disadvantage of EVs is the low energy density possessed by chemical batteries, which ranges around 1% of combustible fuels (Ehsani and Emadi 2005). This characteristic makes EVs applicable for a very specific usage of short range drive. In this case the cost trade-off for the different component configurations and size is off course a major issue.

The main purpose of a hybrid electric vehicle (HEV) in terms of fuel efficiency is to overcome the typical losses of conventional powertrains by accomplishing the following principles:

- Usage of electric motor for propulsion at low speeds and low power requests
- Internal combustion engine (ICE) deactivation when vehicle is stopped
- Regeneration of energy during braking events
- Optimization of engine operation region during mechanical only traction and when in generator mode

Different drivetrain configurations for HEVs can accomplish the task of minimizing fuel consumption. Series-parallel hybrids are well known for providing different modes of operation allowing either pure electrical, pure mechanical propulsion or a combination of both. The powertrain configuration of this study is a series-parallel electric hybrid which uses a planetary gear set as torque-split device by interconnecting ICE and two electric motors. In order to study the operation of this system, a detailed mathematical model was built in MATLAB/Simulink. For this system a non-optimal control strategy was implemented using rule-based control and a charge sustaining strategy. The results of this model were correlated with data from dynamometer testing in order to assure the quality of the powertrain and control model.
The main step of the problem of minimizing fuel consumption consists in finding the optimum power-split between ICE and battery power for a given driver's request. Dynamic programming (dp) uses Hamilton-Jocobi-Bellman equation to solve the problem and find the global optimum solution and has a suitable application for motor vehicles. The use of dynamic programming for the HEV problem is well described in the literature (Lin, Peng, Grizzle, and Kang 2003; Delprat, Lauber, Guerra, and Rimaux 2004) where the accumulated fuel consumption over a driving cycle is used as cost function with addition of a penalty term due to final variation of battery state of charge (SOC). Dynamic programming requires prior information of the driving cycle and, therefore, the simulation is run in backward mode. Moreover, a simplified model representing the dynamic system has to be used which may create a response that deviates from the detailed model using non-optimal control. The time step size and sampling of state and control variables are also factors

that can impact in the results of the optimization. For these reasons, there is the need of having two different models using optimum and non-optimum control.

2. DESCRIPTION OF THE POWERTRAIN SYSTEM

The configuration of the powertrain is shown in Figure 1 where a planetary gear set is used to connect motor-generator 1 (MG1), ICE and motor-generator 2 (MG2) to solar, carrier and ring gears, respectively. The ring gear is connected through the differential and final reduction to the wheels. The ratio of torque amplification from the ICE to the wheels is fixed, however, different ICE speeds can be realized for a given vehicle speed. This is possible by controlling MG1 speed so that it compensates for the ICE torque transferred to the shaft of the solar gear. The main traction motor is MG2, which is also the responsible for regenerative braking.

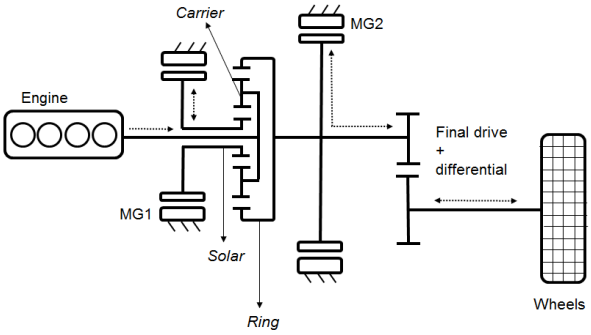

Figure 1: Diagram Of The Power-Split Hybrid Topology With Energy Flow Defined By Arrows.

The 2nd generation of Toyota Prius is used as base from where the main parameters were taken for this study. Data available for this powertrain is widely literature in the literature (Sekimori 1998; Kamiya 2006; Abe 2000). The lever diagram in Figure 2 shows different operation modes of the powertrain. At low speed driving, the traction motor speed is increased while the engine remains stopped with the generator accelerating in the reverse direction (red line). At higher vehicle speeds and loads, the generator accelerates towards the positive direction in order to start the engine (green line). The engine can also operate in fuel cut off and drag along the planetary, with the effect of engine friction lowered due to the overdrive ratio to the wheels. The engine can still be started at standstill in order to generate electricity or in order to warm-up the exhaust system.

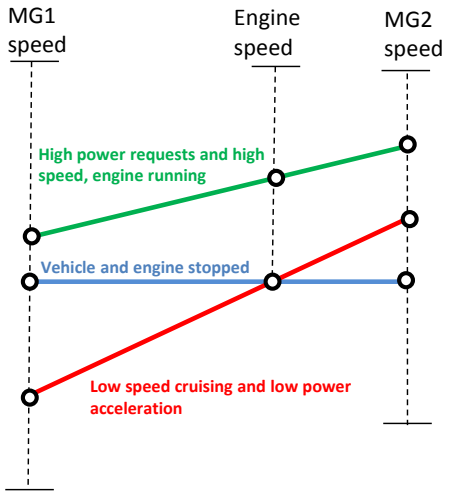

Figure 2: Lever Diagram Of The Power-Split Device.

Table 1: Characteristics of the vehicle model.

Engine	
Displacement	1.5 cm³
Torque	115 Nm @ 4200 rpm
Power	57 kW @ 5000 rpm
Traction motor	
Type	Brushless Permanent Magnet motor
Torque	400 Nm
Power	50 kW
Maximum speed	6500 rpm
Generator	
Type	Brushless Permanent Magnet motor
Power	30 kW
Maximum speed	10000 rpm
Battery	
Type	Ni-MH
Nominal voltage	201.6 V
Rated capacity	6.5 Ah

An inherent feature of the power-split powertrain is that electrical energy is always consumed in order to control engine speed by MG1 attached to the sun gear. As explained in (Abe 2000; Muta, Yamazaki, and Tokieda 2004) at certain vehicle speeds where the engine has to be started, MG1 has negative speed and has to decelerate in order to start the engine, therefore generating energy which is used by the traction motor for torque assist. However, when the engine has to be started at low speeds, MG1 operates as a motor and afterwards uses traction power to control engine speed. At this point, MG2 has to operate as a generator decreasing torque at the output shaft. This constant recirculation of energy on the high voltage bus is beneficial for city driving, where electric traction is

more efficient, so that the energy is not directed in and out of the battery, consequently reducing conversion losses. On the other hand, on highway driving the overall efficiency is reduced as mechanical only traction is not possible. The general characteristics of the vehicle are shown in Table 1.

3. SYSTEM MODELLING

The power-split configuration shown in Figure 1 allows the system to operate as an electric continuous variable transmission (CVT), as the generator is used to control the ICE speed. The torque relationship in the planetary carrier is fixed by the ratio between the diameters of each gear and a general gear ratio of the planetary gear set, i_{PGS}, is defined as the ratio between the number of teeth of ring and sun gears. The dynamic equations for the system are shown in Eq.(1) and Eq.(2), where subscripts C, S, R, represent carrier, sun and ring gear parameters. The torque demand of ICE, MG1 and MG2 described by T_{ICE}, T_{MG1} and T_{MG1} are related to the torque demanded at the wheels. Inertia terms from the planetary are represented by I_S, I_R and I_C, while $I_{ICE}/\alpha_{ICE}, I_{MG1}/\alpha_{MG1}$ and I_{MG2}/α_{MG2} represent inertia and angular acceleration of ICE, MG1 and MG2, respectively. The equivalent rotational inertia of the vehicle mass on the ring shaft is represented by I_{R-EQ}.

$$T_{MG1} - I_S\alpha_{MG1} = -\left(\frac{1}{i_{PGS}+1}\right)\cdot\left(T_{ICE} - I_C\alpha_{ICE}\right) \quad (1)$$

$$\left(\frac{i}{i_{PGS}+1}\right)\cdot\left(T_e - I_{ICE}\alpha_{ICE}\right) + T_{MG2} - I_R\alpha_{MG2} =$$

$$= \frac{T_{W-R}}{i_{MG2-wheel}} - I_{R-EQ}\alpha_{MG2} \quad (2)$$

The ratio of the planetary gear set of the system under study is 2.6, meaning that 72% of engine torque is transferred to the driveshaft and 28% to the electric generator at any condition. This is in line with the equations above. A comparison to a manual transmission can be made such that in this case the engine has an overdrive gear ratio to the wheels. The ratio of angular speed between the sun, carrier and ring gear is derived by the following equation:

$$(i_{PGS}+1)\cdot\omega_{ICE} = \omega_{MG1} + i_{PGS}\cdot\omega_{MG2} \quad (3)$$

The equation above indicates that there are two independent variables in the system, therefore, for a given wheel speed there will be a number of possibilities for engine and generator speeds. In this way, MG1 will be responsible for controlling the engine speed and electrical power will likely to always be consumed when the engine is on. From Eq. (1), MG1 will always have a negative torque in order to control the ICE speed in a constant level but exceptions can happen in case of transients of engine speed.

4. VEHICLE PLANT MODEL

The ICE model does not incorporate thermo-mechanical or combustion phenomena, therefore, behaviors during catalyst and coolant warm-up are neglected. The model works with an external torque request for the ICE from the main control strategies and incorporates the maximum torque limitation across speed, a friction model and idle controller. Engine friction is based on the model proposed by Chen and Flynn (1965) where the resistance load is subject to a constant term, and two terms dependent on the rotational speed and its square.

An important aspect of the simulation with impact on the fuel economy is the efficiency map of the engine. Duoba, Ng, and Larsen (2000) a torque sensor was added to the engine output shaft and torque measurements were executed in the vehicle at steady state speeds. The results, however, don't cover the whole operation range of the engine, instead, only the points resultant from the control strategy.

In order to reproduce the efficiency map of the engine, a thermodynamic engine model was created in the GT-Power software and combustion characteristics where calibrated throughout the engine speed and torque in order to result in the brake specific fuel consumption map (BSFC) shown in Figure 3. The optimum operation line (OOL) for this efficiency map is also shown in the graph and it presents a high correlation to the OOL presented by Kim, Rousseau, and Rask (2012) from real vehicle testing.

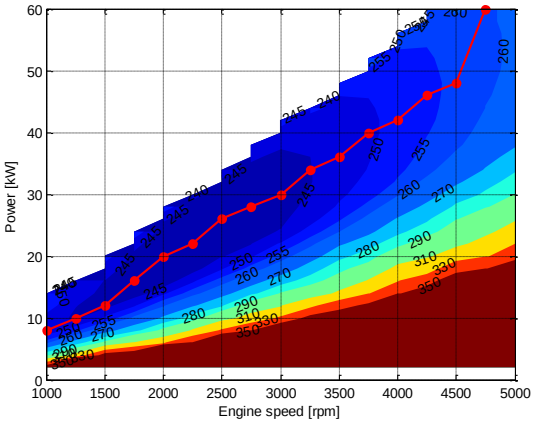

Figure 3: Engine BSFC Map And Optimum Operation Line.

Regarding ICE start and shutdown behavior, (Duoba, Henry, and Larse 2001; Ayers, Hsu, Marlino, Miller, Ott, and Oland 2004) show test results with a maximum acceleration of 4000rpm/s during startup and -2000rpm/s during shut down. Those are important parameters for determining the ICE start torque from MG1.

The model of traction motor and generator incorporates the torque limitation characteristics of each motor with a look-up table. An investigation was conducted by (Hsu, Nelson, Jallouk, Ayers, Campbell, Coomer, Lowe, and Burress 2005) in order to determine the

continuous torque values of the traction motor that produces a limited winding and oil temperature for a certain inlet coolant temperature. Results show a continuous torque of 167Nm for an inlet coolant temperature of 34.6˚C. Moreover, the peak rated capacity generates a rise in winding temperature of 2.1 °C/s.

From the OOL in Figure 3, which produces a fixed relation between engine speed and torque, the system from Eq. (3) is reduced to only one degree of freedom. For the transmission model, the losses were incorporated from (Ayers, Hsu, Marlino, Miller, Ott, and Oland 2004) which shows a maximum total system loss of 2500W at 170 km/h.

5. BATTERY MODEL

The battery model is simulated using a capacitor as voltage source with internal and parasitic losses. As shown in Ehsani and Emadi (2005), the terminal voltage of such a battery is defined as:

$$V_T = V_{OC} - R_i \cdot I \tag{4}$$

Where V_{OC}, R_i and I are the open circuit voltage, internal resistance and terminal current, respectively. The sum of terminal current and leakage current of the battery can be expressed as:

$$I + I_L = -C\frac{dV_{OC}}{dt} \tag{5}$$

Where C is the capacitance of the battery. The leakage current is defined by V_{OC} / R_L and, when substituted in Eqs (4) and (5), leads to:

$$\frac{dV_{OC}}{dt} = -\left(\frac{V_{OC}}{CR_L} + \frac{I}{C}\right) \tag{6}$$

The resultant battery model in Simulink from this system of equations is shown in Figure 4. The electrical circuit is shown in Figure 14 from the Appendix.

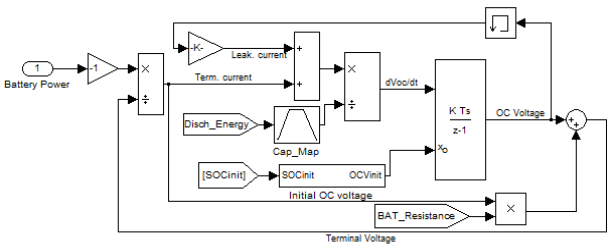

Figure 4: Battery Model In Simulink.

The validation of the battery model was done against data from tests performed by Gray and Shirk (2010) in which the battery was discharged with a constant rate of 1C (Figure 15 from the Appendix). The value used in the validation corresponds to a new battery. The battery capacity was then calibrated in order to match the test data. The resulting battery terminal voltage of the validation model is shown in Figure 5.

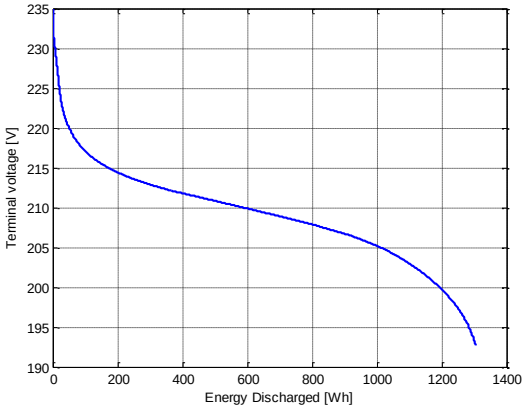

Figure 5: Validation Of The Battery Model.

6. DRIVER MODEL

The main function of the driver model is to set the desired traction torque target to be used in the forward simulation. This model contains a PID controller which compares the target speed from the input driving cycle to the actual vehicle speed. The output of the PID is the torque demand on the driveshaft, which is directly proportional to the accelerator pedal request. The driver model performance is such that the difference between followed and targeted vehicle speed must lie within a margin of 1 km/h. Figure 6 shows the difference between target and simulated speed for the NEDC cycle. The absolute difference throughout the cycle is below 0.3 km/h which indicates proper modelling not only for the driver model but also for the complete powertrain control system.

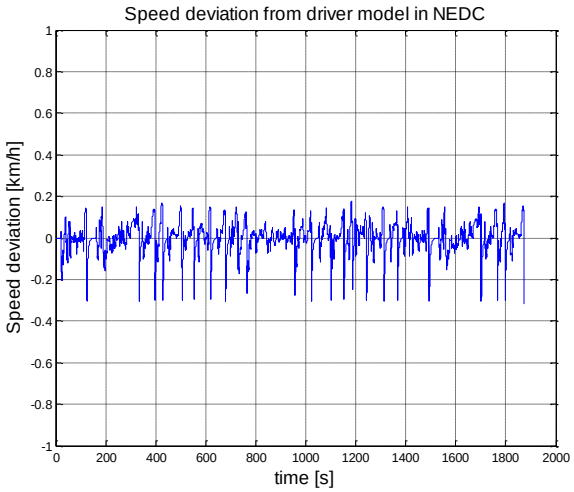

Figure 6: Absolute Speed Error From PID In Driver Model.

7. TEST DATA

Data from tests performed with Toyota Prius Gen 3 are available from Argonne National Laboratory (2013). Although the powertrain configuration has small

differences in comparison with the one presented here, the data provides a good base for validating the system. These data correspond to chassis dynamometer testing of the vehicle operating under the urban cycle FTP75.

8. GENERAL GUIDELINES

The basis for the control system design relies on the test measurements described below. The graph of Figure 7 shows the driver's request power at which the engine is turned on during the driving cycle. One can see that the ICE usually starts in a region between 8kW and 9kW.

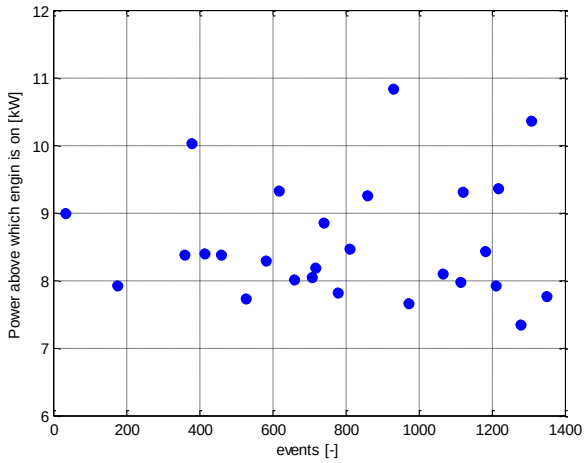

Figure 7: Engine-On Condition From Test Data.

When the engine is running, it should provide the full power demand of the road plus the battery power demand. The battery power demand is shown in Figure 8 where additional power is added to the ICE power demand in order to charge the battery when the SOC is low, or to help discharging the battery in case SOC is high. This strategy was observed by Kim, Rousseau, and Rask (2012) during vehicle tests.

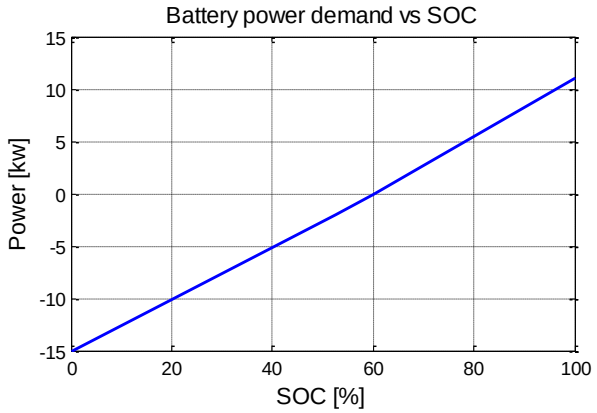

Figure 8: Battery Power Demand Added To Engine Power.

9. SIMULATION RESULTS

As mentioned before, the simulation runs in forward mode with the load request set by the driver model. Figure 9 shows vehicle and ICE speed for the simulation and test data results under the FTP75 cycle. At this point, no emission strategy is considered what makes the ICE operates with start stop profile in the beginning of the cycle. The results show that even at speeds around 50 km/h, the traction is purely electrical and the engine basically assists the vehicle during accelerations and high speed cruising. One constrain is that above 68 km/h the engine has to be turned on in order to prevent the generator speed becoming too high, what would lead to little torque reserve to perform an engine start.

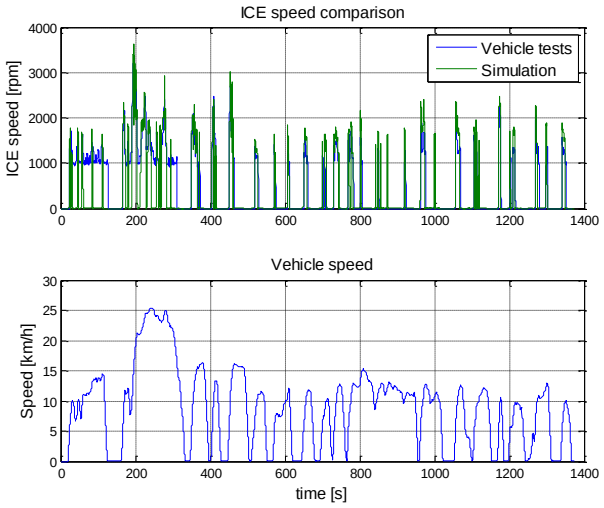

Figure 9: Results For ICE Speed.

Battery SOC and fuel consumption are shown in Figure 10, in this case for the extended FTP75 cycle, which includes the initial 500s of the cycle again at it's end. The net change in SOC at the end of the cycle was around -1%, which means that the compensated fuel consumption should be slightly higher. The final value of the non-corrected fuel economy of the simulation is 2.93l/100km which is close to the experimental data of 3.11l/100km with hot engine and 3.73l/100km with a cold engine. In the tests from Argonne National Laboratory (2013), the net variation of integrated battery current is very close to zero.

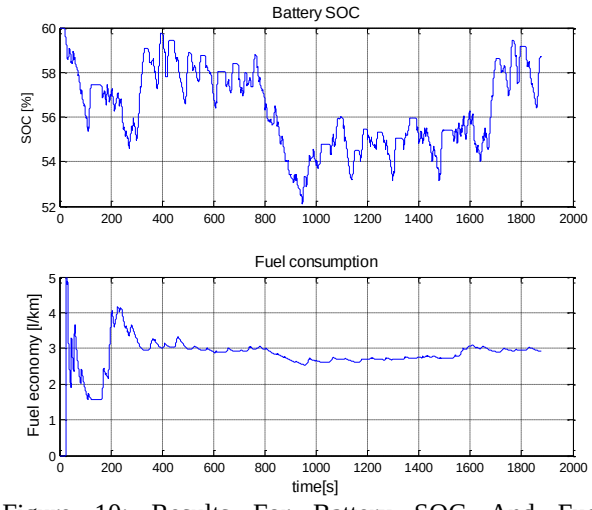

Figure 10: Results For Battery SOC And Fuel Consumption.

10. OPTIMAL CONTROL

Dynamic programming is an optimization algorithm which aims to finding the solution that generates the global minimum result for a determined cost function. This means that for a given driving cycle, the optimized solution will be a vector of control values against time. A time continuous function represent the current system can be represented by:

$$\dot{x}(t) = f(x(t), u(t), t) \tag{9}$$

where u(t) is the control variable, in this case the power-split (PS), and x(t) is the vector of state variables of the system, in this case the battery SOC. The cost function for this system is:

$$J(u(t)) = G(x(t_f)) + \int H(x(t), u(t), t)dt \tag{10}$$

where $G(x(t_f))$ is the final cost and the second term represents a penalty to ensure that a dynamic constrain should be satisfied, in this case that the SOC at the beginning and at the end are the same. The following cost function represent the fuel consumption in the vehicle over the driving cycle:

$$J(u(t)) = \int \dot{m}_{fuel}(u(t), t)dt \tag{11}$$

The constrains for the optimization have to be set in order to prevent that the system drift out of its boundaries:

$$T_{\min} < T_{req} < T_{\max} \tag{12}$$

$$SOC_{\min} < SOC < SOC_{\max} \tag{13}$$

$$SOC_{end,\min} < SOC_{end} < SOC_{end,\max} \tag{14}$$

$$u_{\min}(SOC, t) < u(SOC, t) < u(SOC, t)_{\max} \tag{15}$$

where T are torque requests in the system for all three power sources and SOC_{end} represent the variation of SOC from beginning to the end of the cycle.

The DP routine developed by Sundström and Guzzella (2009) was used in this analysis. The range of the PS control variable was divided in 0.1 intervals from [-1, 1], where 1 means pure electric, values between 0 and 1 mean electric assist drive, 0 means pure ICE traction, and negative values mean electric generation (no electric assist drive). The moment of ICE start could also have been inserted as a control variable but was made the same as in the detailed model. The SOC was divided in 61 steps between the range of 50% to 70% where it is allowed to vary. The constraint on the final SOC is a net variation of 1% against the initial SOC.

The detailed model in Simulink is not appropriate to this optimization due to the increase of computational power that would be necessary and also due to the difficulty of implementation. A backward looking simplified model was therefore implemented. It incorporates the same efficiency maps for the power sources of the model presented above and has a 1s time step while the detailed model runs at 0.01s.

Figure 11 shows the PS result of the DP algorithm corresponding to the ratio of traction power from MG1 and MG2 by total power demand. The first graph shows the dependency against power demand at wheels. The traction is purely electrical until around 8kW (PS = 1), between 8kW and 12kW there is no assist drive but only charging (negative values of PS), which means that the ICE power is increased in order to go to higher efficiency islands. At further higher power values, the ICE is also set to generate in most of the events with very few events of electric assist (1 < PS < 0). The second graph of PS against vehicle speed shows similar results with the trend of having limited generation at higher speeds towards a pure ICE traction.

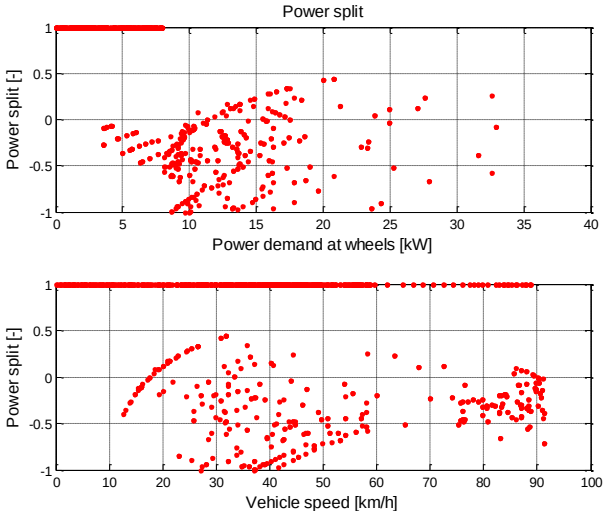

Figure 11: Power-Split (Control Variable) Result From The Dynamic Programming.

The fuel consumption result from the DP was 3.73l/km which is higher than the result of the detailed model, 2.93l/100km, with non-optimal control. Figure 12 shows battery power for a section of the driving cycle resultant from the detailed model and DP. Peaks around 25kW correspond to engine start events which take around 0.4s (Duoba, Henry, and Larse 2001). Although the trend of both curves is similar, one can see that the major differences come from the coarse time step size of 1s used in the DP routine. Behaviors such as engine start are then not taken into account as they happen in a smaller time frame. As a consequence, the total energy demand at the driveshaft and the results of the PS present high deviation when compared to the detailed model.

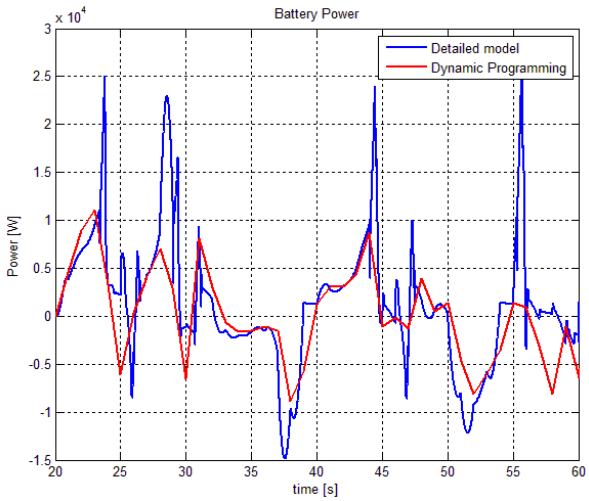

Figure 12: Battery Power For Detailed Model And DP.

The main task of the dynamic programming was building a PS map where the intended distribution of power between ICE, MG1 and MG2 could be optimally scheduled. The behavior of the state variable is shown in Figure 13 and it tells the response of the system to the variations in the control input variable.

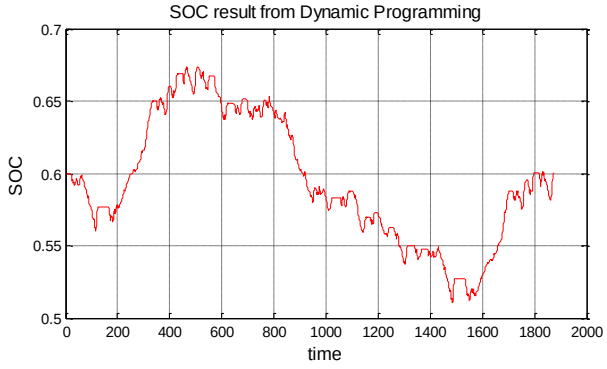

Figure 13: Dynamic Programming Result For SOC (State Variable).

11. CONCLUSION AND FUTURE WORK

Due to the differences between detailed model and the DP model, comparable results will only be possible when the DP routine runs with similar time step sizes as the detailed model. Until now this was not possible due to exponential increase in computational load and time required for convergence in the DP routine. Other optimal control programs could be used and this will be investigated further. The dynamic programming routine should be adapted so that it also decides on the moment that the ICE should be turned on. For a practical application of the results from the DP, either local optimization or a look-up table based control would have to be implemented in the detailed model as the implementation of DP in real-time is not possible.

ACKNOWLEDGMENTS

The authors greatly appreciate the data made available by Argone National Laboratory. Without this data, the validation of the vehicle model and control strategy would not be possible. Also, the DP routine made available by ETH and Olle Sundström was of essential contribution.

APPENDIX

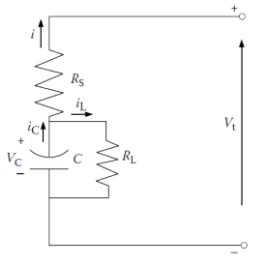

Figure 14: Equivalent Battery Circuit. Courtesy Of Ehsani and Emadi (2005).

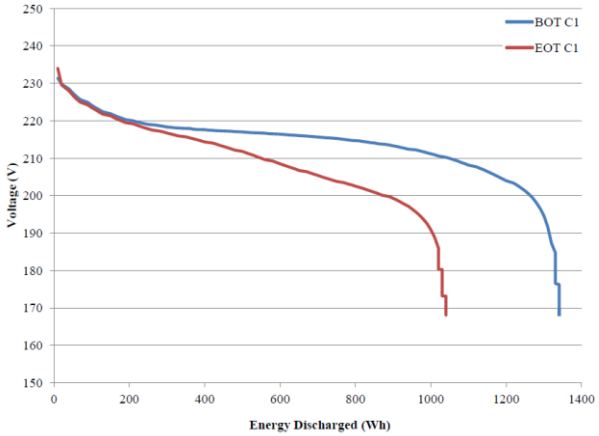

Figure 15: Voltage Variation During Battery Discharge Tests (BOT indicates new battery, EOT indicates used battery). Courtesy Of Gray and Shirk (2010).

REFERENCES

Ehsani M., Gao Y., Emadi A., 2005. Modern Electric, Hybrid Electric, and Fuel Cell Vehicles, Fundamentals, Theory, and Design. 2nd ed. Florida: CRC Press.

Lin C., Peng H., Grizzle J., Kang J., 2003. Power management strategy for a parallel hybrid electric truck. IEEE Trans. Control Systems Technol., 11(6), 839–849.

Delprat S., Lauber J., Guerra T., Rimaux J., 2004. Control of a parallel hybrid powertrain: Optimal control. IEEE Transactions on Vehicular Technology, 53(3), 872–881.

Sekimori T., 1998. Development of Toyota's Electric and Hybrid Vehicle. SAE Technical Paper 98C053, 355-361.

M. Kamiya, 2006. Development of traction drive motors for the toyota hybrid system. IEEE Transactions on Industry Applications, 126(4), 473-479.

Abe S., 2000. Development of the Hybrid Vehicle and its Future Expectation. SAE Technical Paper 2000-01-C042.

Muta K., Yamazaki M., Tokieda J., 2004. Development of New-Generation Hybrid System THS II -

Drastic Improvement of Power Performance and Fuel Economy. SAE Technical Paper 2004-01-0064.

Duoba M., Ng, Henry, Larse R., 2001. Characterization and Comparison of Two Hybrid Electric Vehicles (HEVs) – Honda Insight and Toyota Prius. SAE Techinical Paper 2001-01-1335.

Rask E., Duoba M., Busch H., Bocci D., 2010. Model Year 2010 (Gen 3) Toyota Prius Level-1 Testing Report. Argonne National Laboratory. Report ANL/ES/RP-67317.

Chen S. and Flynn P., 1965. Development of a Single Cylinder Compression Ignition Research Engine. SAE Technical Paper 650733.

Duoba M., Ng H., Larsen R., 2000. In-Situ Mapping and Analysis of the Toyota Prius HEV Engine. SAE Technical Paper 2000-01-3096.

Kim N., Rousseau A., Rask, E., 2012. Autonomie Model Validation with Test Data for 2010 Toyota Prius. SAE Technical Paper 2012-01-1040.

Hsu J.; Nelson S., Jallouk P., Ayers C., Campbell S., Coomer C., Lowe K., Burress T., 2005. Report on Toyota Prius motor thermal management. Oak Ridge National Laboratory, ORNL/TM-2005/33.

Gray T., Shirk M., 2013. Toyota Prius VIN 0462 Hybrid Electric Vehicle Battery Test Results. Idaho National Laboratory INL/EXT-13-28025.

Ayers C., Hsu J., Marlino L., Miller C., Ott Jr.G., Oland C., 2004. Evaluation of 2004 Toyota Prius Hybrid Electric Drive System Interim Report. ORNL/TM-2004/247.

Argonne National Laboratory, 2013. All Data- 2010 Toyota Prius, Available from: http://www.anl.gov/energy-systems/group/downloadable-dynamometer-database/hybrid-electric-vehicles/2010-toyota-prius, [Accessed 17 February 2015].

Sundström O., Guzzella L., 2009. A Generic Dynamic Programming Matlab Function. Proceedings of the 18th IEEE International Conference on Control Applications, 1625–1630, Saint Petersburg, Russia.

AUTHORS BIOGRAPHY

Agenor de Toledo Fleury has a degree in mechanical engineering from ITA - Technological Institute of Aeronautics (1973), a MSc (1978) and a PhD degree in Mechanical Engineering from the University of São Paulo (1985). He is currently full-time professor at FEI University and a part-time PhD professor at Polytechnic School, University of Sao Paulo. He has led various projects with emphasis on Dynamics and Control Systems. His most recent projects address modeling and control of nonlinear systems, optimal control and estimation, in applications of Biomechanics, Robotics and Automotive Engineering.

Ivan Miguel Trindade is a Master student at Polytechnic School of University of São Paulo and has a degree in mechanical engineering (2008) from the same university. He has worked on various projects with internal combustion engine and hybrid powertrain development. Nowadays he works in Punch Powertrain N. V. with control systems development for hybrid and electric powertrains.